3D DEM simulations of triaxial compression tests of cemented sandstone

A.K. Rakhimzhanova, F.A. Khamitov & N.H. Minh

Nazarbayev University, Astana, Kazakhstan

C. Thornton

University of Birmingham, Birmingham, UK

ABSTRACT: Three-dimensional DEM simulations of triaxial compression tests on loose samples, using periodic boundaries, were performed using 5206 frictional elastic spheres at different values of confining pressure and bond strength. The results show that the peak strength and stiffness depend on the bond strength. For a higher bond strength, the material becomes stiffer and the peak stress is reached at a lower strain; the sample exhibits a higher volumetric dilation and less bond breakage. Bond breakage was found to increase with confining pressure. The Mohr-Coulomb strength parameters c' and φ' were obtained for the numerical samples and correlations between the shear strength parameters and the bond strength were established. The correlations were then used to identify the bond strength to be used for comparisons with experimental results. The stress-strain responses of the numerical samples were found to be in good agreement with the experimental results of the cemented sandstone.

1 INTRODUCTION

The behaviour of the reservoir sandstone from the Ustyurt-Buzachi Sedimentary Basin had been studied using analogue samples and laboratory triaxial compression test by Shabdirova et al. (2016) and it was found that failure and deformation of the material are dependent on the cement bonds but the experimental study was very limited in term of studying the bond breakage behaviour.

In the last decade, bonded granular material has been numerically studied using the Discrete Element Method (DEM) proposed by Cundall & Strack (1979). Wang et al. (2008) experimentally and numerically (2D) examined the material behaviour of cemented sand using triaxial compression tests; Jung et al. (2012) numerically (3D) studied the stress-strain response of hydrate-bearing sand. Utili & Nova (2008) presented a 2D contact model for bonded granular materials based on the Mohr-Coulomb failure criteria; Obermayr et al. (2013) proposed 3D bonded-particle model for cemented sand, where the centres of spherical particles are connected by elastic beams; Shen et al. (2016) presented a 3D bonded contact model and its application to cemented sand and to grain-coating type methane hydrate bearing sand (Shen & Jiang 2016).

The paper presents a 3D bond contact model for cemented sandstone and reports results obtained from 3D DEM simulations of triaxial compression tests on loose samples of cemented sand in periodic cells.

2 CONTACT BOND MODEL

The so-called JKR model of adhesion was proposed by Johnson et al (1971) to model autoadhesive interactions due to van der Waals forces between silt sized particles. However, the oil field reservoir rock is sandstone, i.e. sand with cement bonds. Nevertheless, in the simulations reported here we used a simple modification of the JKR model for the normal contact force and the Mindlin (1949) no slip model for the tangential contact force. The normal force displacement curve for JKR theory was provided by Johnson (1976) and is illustrated in Fig. 1.

When two particles come into contact ($\alpha = 0$) the normal force F_n immediately drops down to point A due to van der Waals attractive forces. During the compression (loading stage) the normal contact force increases from point A to say point B. If decompression (unloading) then occurs the response is elastic and the force returns from point B to point A, where the value of relative approach is $\alpha = 0$, but there is still a finite area of contact. All the work that was done during the loading stage will be recovered when the normal contact force reaches point A during unloading. At point A the spheres remain adhered together, and extra work is required to break the contact. During the extra work the tensile force increases from point A to point C and then decreases until contact breaks at point D.

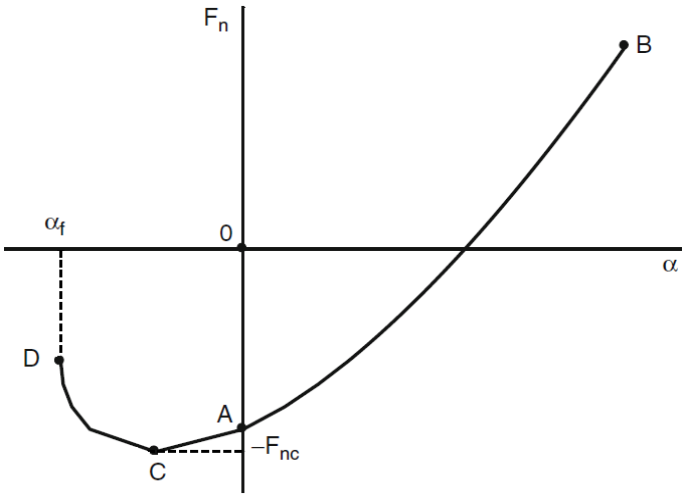

Figure 1. Normal force-displacement curve.

Cement bonds are not as stretchable and break in a brittle manner. Consequently, in the modified JKR model used in this research the bond breaks at point C and any subsequent new contact will be treated as non-adhesive with the normal contact force calculated by Hertzian theory. At point C, the maximum tensile force required to break the contact is:

$$F_{nc} = 1.5\pi\Gamma R^* \quad (1)$$

where Γ is the interface energy and $1/R^*$ is the relative curvature of the contact defined as:

$$\frac{1}{R^*} = \frac{1}{R_1} + \frac{1}{R_2} \quad (2)$$

3 NUMERICAL SIMULATIONS

Three-dimensional simulations of triaxial compression tests on loose samples, using periodic boundaries, have been performed using 5206 frictional elastic spheres at different values of confining pressure and bond strength. Following Calvetti & Nova (2004), the spheres were prevented from rotating in order to obtain reasonable values of shear strength.

3.1 *Specimen generation*

The particle size distribution (PSD) data of the sandstone analogue samples from the Ustyurt-Buzachi Sedimentary Basin measured by Qicpic dynamic image analyser (Shabdirova et al. 2016) was replicated with the numerical samples (Fig. 2).

Eight different particle sizes were randomly generated within a cuboidal cell of dimension 4.25 mm: 0.15 mm (614), 0.18 mm (911), 0.2 mm (783), 0.22 mm (811), 0.25 mm (1027), 0.275 mm (583), 0.3 mm (318) and 0.355 mm (159). The following mechanical properties were selected: Young's modulus E = 70 GPa and Poisson's ratio ν = 0.3.

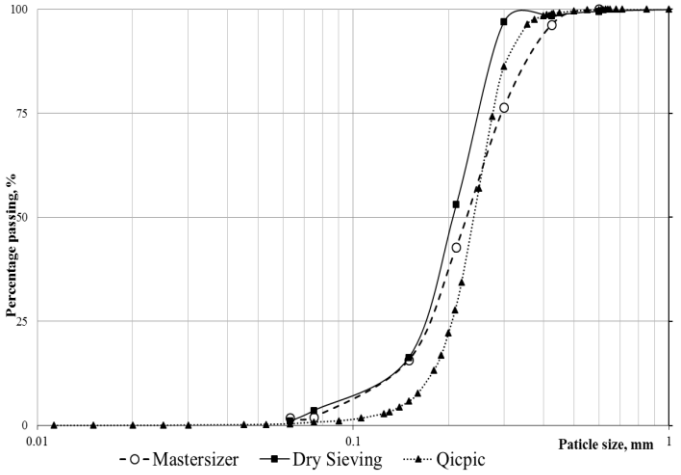

Figure 2. Particle Size Distribution of the reservoir sand from the Ustyurt-Buzachi Sedimentary Basin

The interparticle friction coefficient was set to μ = 0.3 during the particle generation stage in order to obtain a loose sample. The experimental particle density ρ = 2605 kg/m^3 was used but scaled up by a factor of 10^{12} in order to model quasi-static simulations within a reasonable timescale. Thornton (2000) reported that the particle density scaling does not affect forces and displacements and hence stresses and strains; the velocities and accelerations are reduced by orders of magnitude but these are not of concern when considering quasi-static behaviour. Contact damping was used and the normal and tangential damping forces were calculated as:

$$F_{nd} = 2\beta\sqrt{m^* k_n}\Delta\alpha/\Delta t \quad (3)$$

and

$$F_{td} = 2\beta\sqrt{m^* k_t}\Delta\delta/\Delta t \quad (4)$$

where

$$\beta = \frac{frac}{2\pi \cdot freq} \quad (5)$$

with the Rayleigh damping parameters chosen to be fraction = 0.05 and frequency = 0.5. However, following Cundall & Strack (1979), the contact damping forces do not contribute to the stored contact forces, only to the out-of-balance force on the particle, from which the particle acceleration is obtained.

3.2 *Isotropic and triaxial compression*

After generation, isotropic compression was carried out to the desired mean stress to prepare the system for subsequent shear deformation. Numerical servo-control algorithms were used to control the isotropic compression stage and to maintain $\sigma_3 = \sigma_2$ constant during the shear stage (Thornton 2000). A total of 20 simulations were performed over a range of confining pressures of 100, 300, 500 and 1000 kPa and bond strengths (interface energy of adhesion) of Γ = 0, 10, 20, 30 and 40 J/m^2, where Γ = 0 J/m^2 is an uncemented sample. In all simulations, the sample was isotropically compressed to 80 kPa using the Hertzian contact model and then the bond strength was introduced at 80 kPa. The initial number of bonds was equal to 7526 for all samples. During further isotropic compression and throughout the shear stage the modified JKR model was used for bonded contacts but for any new contacts that may be created the Hertzian model was applied.

4 NUMERICAL RESULTS

4.1 *Macroscopic response*

Figure 3 shows the deviator stress vs. axial strain curves obtained for triaxial compression test simulations at a confining stress of 300 kPa. The results show that both the peak strength and initial stiffness increase with increase in the bond strength; and for a higher bond strength the peak stress is reached at a lower axial strain. Figure 4 shows the effect of bond strength on the evolution of the volumetric strain. All samples first contracted and then started to dilate. For a higher bond strength, the material starts to expand at a lower axial strain and, with increase in bond strength, the sample exhibits a higher rate of dilation.

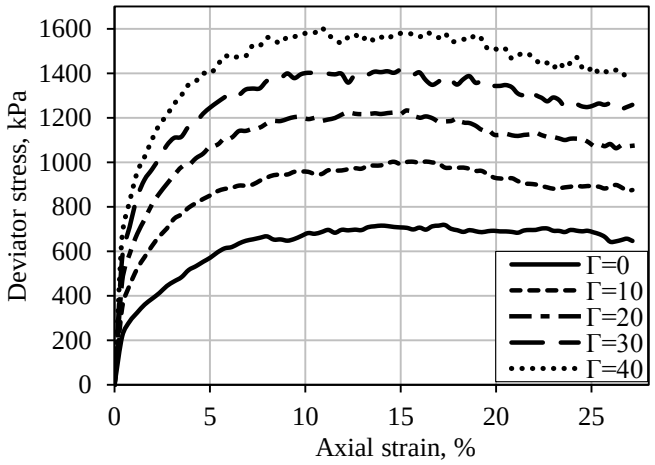

Figure 3. The effect of bond strength on the evolution of the deviator stress.

The results shown in Figs. 3 and 4 are qualitatively typical of all the tests simulated at other confining stresses. In Fig. 3 it is noted that, at the end of the tests, the stress-strain curves for different values of bond strength do not converge. This is because the critical state strength depends on the magnitude of the bond strength, in the same way that it depends on the value of interparticle friction.

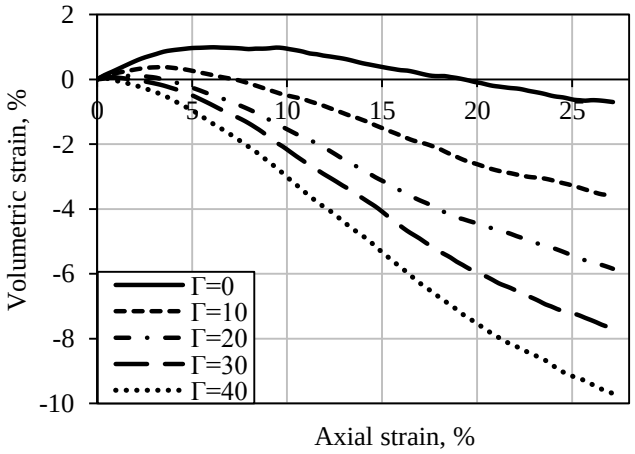

Figure 4. The effect of bond strength on the evolution of the volumetric strain.

4.2 *Microscopic response*

Figures 5 and 6 show the evolution of the number of bonds and the number of contacts, respectively. It can be seen from Fig. 5 that the number of bonds decreases at a decreasing rate and more bonds are broken for a lower bond strength. Figure 6 shows that, for $\Gamma > 0$, the number of contacts initially decreases due the breaking of bonds but then the total number of contacts (both bonded and unbonded new contacts) increases at a decreasing rate. The total number of contacts reduces with increase in bond strength.

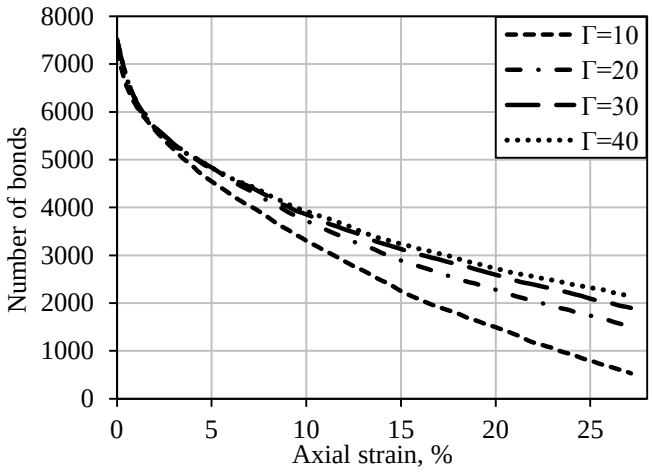

Figure 5. Evolution of number of bonds

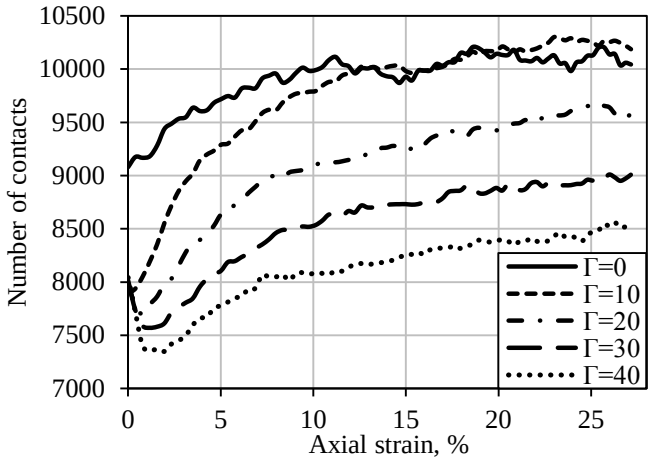

Figure 6. Evolution of number of contacts

5 COMPARISON WITH EXPERIMENTAL DATA

In Fig. 7 the peak strength data obtained from all the simulations are plotted in order to obtain the parameters c' and φ' of the Mohr-Coulomb strength criterion:

$$\sigma_1' - \sigma_3' - 2c'\cos\varphi' - (\sigma_1' + \sigma_3')\sin\varphi' = 0 \qquad (6)$$

where c' = apparent cohesion and φ' = the so-called angle of internal friction. The figure indicates that, according to best fit lines, the friction angle increases slightly with bond strength. Using an average value of 33.7º, the apparent cohesion can be calculated from:

$$c' = \frac{(\sigma_1 - \sigma_3)}{2cos\varphi} - \frac{(\sigma_1 + \sigma_3)tan\varphi}{2} \qquad (7)$$

and the correlation between c' and Γ can be obtained, as illustrated in Fig. 8.

Superimposed on both figures is an experimental data point obtained from laboratory tests on sandstone analogue samples by Shabdirova et al. (2016), which indicates that a value of Γ = 6.5 should be used to compare the numerical simulations with the laboratory results.

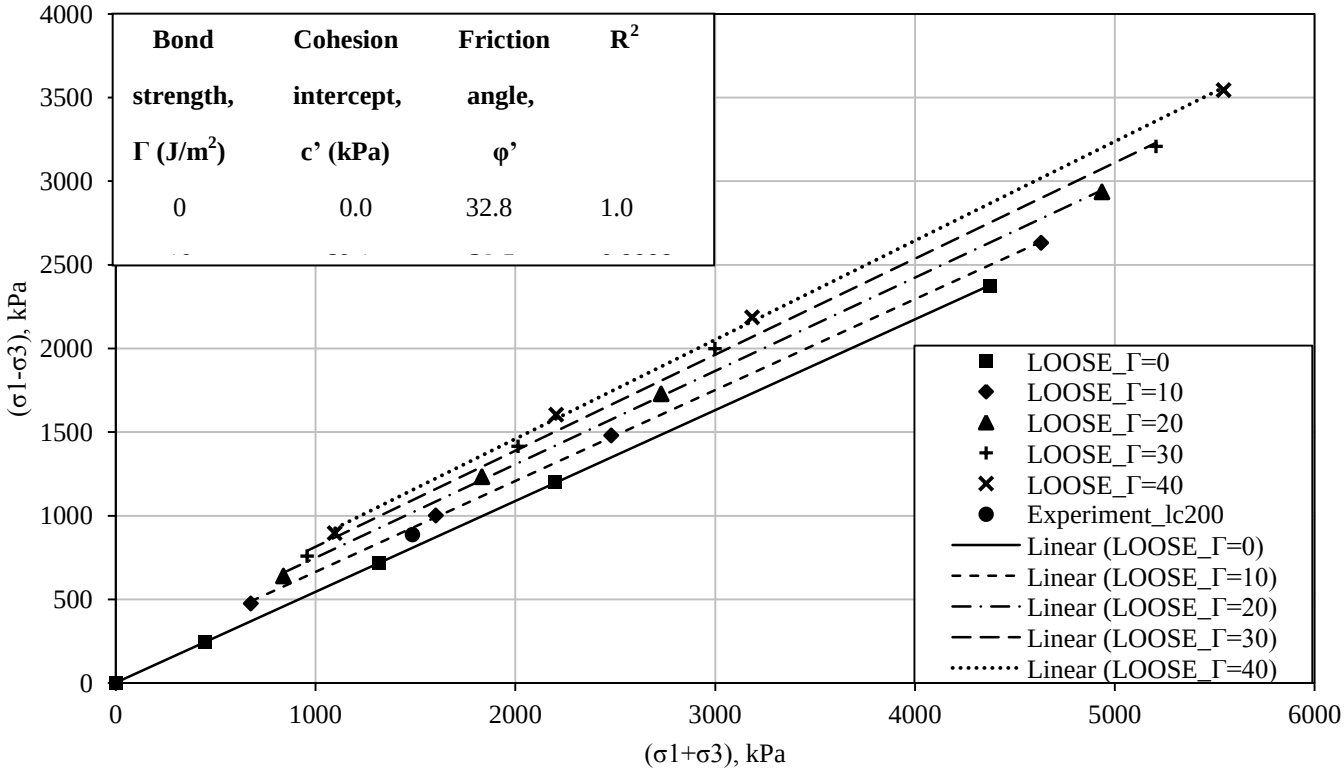

Figure 7. Mohr-Coulomb strength envelopes.

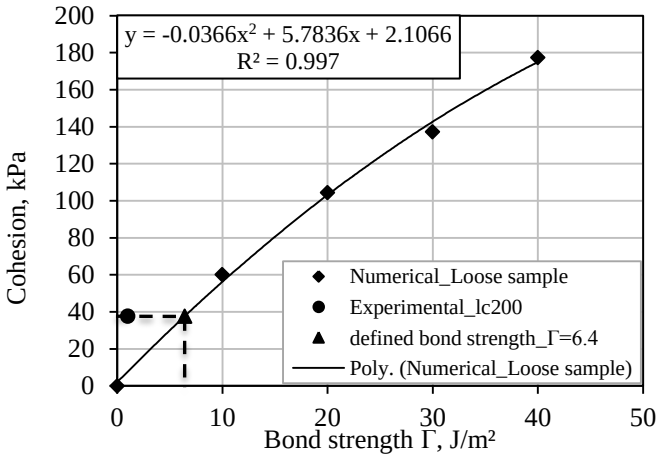

Figure 8. The correlation between the shear strength parameters and the bond strength

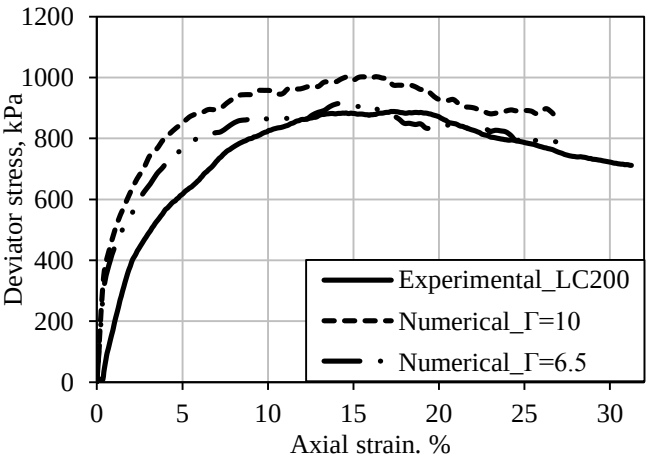

Figure 9. Comparison of numerical and experimental stress-strain curves.

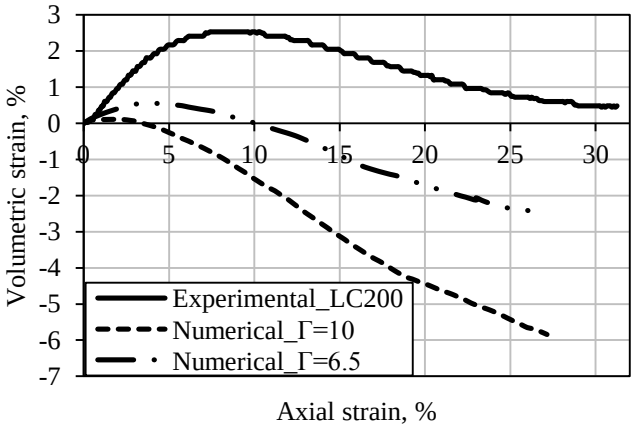

Figure 10. Comparison of numerical and experimental volume change curves.

Figures 9 and 10 show the comparison obtained between the numerical data and a laboratory triaxial compression test at a confining pressure of 300 kPa. It can be seen that, if a bond strength of $\Gamma = 6.5$ J/m^2 is used for the numerical simulation, there is excellent agreement in terms of the peak deviator stress. However, initially, the numerical sample is much stiffer than in the experiment. This is probably due to the fact that there is significantly less initial contraction in the numerical simulation, which may be due to the fact that cement bonds are compressible and this is not accounted for in the simple modified JKR bond model.

6 CONCLUSIONS

In this paper, a 3D bond contact model for cemented sandstone material has been developed by modifying the previous existing JKR theory for auto-adhesive silt size sand particles. In the presented modified JKR contact bond model any new contact after the cement bond breakage will be calculated as non-adhesive. The model parameter is the bond strength in terms of the pseudo interface energy. As an application, 3D DEM simulations of triaxial compression test in periodic cells with the input data of experimental sandstone from the Ustyurt-Buzachi Sedimentary Basin were used. Correlations between the shear strength parameter from the Mohr-Coulomb strength criterion and the bond strength have been provided, which was used to find the value of bond strength to compare the numerical simulation with the experimental result.

The results show that the numerical simulated macroscopic response is in good agreement with the material behaviour of cemented sandstone observed in the real experiment. Consequently, the microscopic response of experimental cemented sandstone material can be examined by numerical results. With increase in bond strength, the peak strength and initial stiffness increase, the sample exhibits a higher rate of dilation and less bond breakage.

ACKNOWLEDGMENTS

This research was supported by the EU Project GEO-RAMP (H2020-MSCA-RISE-2014 GA 645665) and by the Nazarbayev University research grant SOE 2015004. The authors gratefully acknowledge Prof. Stefano Utili (Newcastle University) and Dr. Helen Cheng (University College London) for their help during the first author's visits to the UK.

REFERENCES

Calvetti, F. & Nova, R. 2004. Micromechanical approach to slope stability analysis. *Degradation and Instabilities in Geomaterials.* Springer: Berlin, 235–254.

Cundall, P.A. & Strack, O.D.L. 1979. A discrete numerical model for granular assemblies. *Geotechnique* 29(1): 47-65.

Johnson, K.L., Kendall, K., & Roberts, A.D. 1971. Surface energy and the contact of elastic solids. *Proc. R. Soc. Lond. A.* 324(1558): 301-313.

Johnson, K.L.1976. Adhesion at the contact of solids. In: Koiter, W.T. (ed.) *Theoretical and Applied Mechanics. Proc. 4th IUTAM Congress.*133–143.

Jung, J.W., Santamarina, J.C., & Soga, K. 2012. Stress-strain response of hydrate-bearing sands: numerical study using discrete element method simulations. *Journal of Geophysical research* 117: 1-12.

Mindlin, R.D.1949 Compliance of elastic bodies in contact. Trans. ASME *J. Appl. Mech.* 16, 259–268.

Obermayr, M., Dressler, K., Vrettos, C. & Eberhard, P. 2013. A bonded-particle model for cemented sand. *Computers & Geotechnics* 49: 299-313.

Shabdirova, A.D., Bissekenova, Z., Minh, N.H., & Kim, J.R. 2016. Sample preparation method of clay-rich sandstone analogue reservoir in Kazakhstan. *50th Rock Mechanics/Geomechanics Symposium,* Houston, Texas.

Shen, ZF. & Jiang, M. 2016. DEM simulations of bonded granular material. Part II: Extension to grain-coating type methane hydrate bearing sand. *Computers and Geotechnics* 75: 225-243.

Shen, ZF., Jiang, M. & Thornton, C. 2016. DEM simulations of bonded granular material. Part I: Contact model and application to cemented sand. *Computers and Geotechnics* 75: 192-209.

Thornton, C. 2000. Numerical simulations of deviatoric shear deformation of granular media. *Geotechnique* 50(1): 43-53.

Utili, S. & Nova, R. 2008. DEM analysis of bonded granular geomaterials. *International Journal for Numerical and Analytical Methods in Geomechanics* 32(17): 1997-2031.

Wang Y.H. & Leung S.C. 2008. Characterization of cemented sand by experimental and numerical investigations. *Journal of Geotechnical and Geoenvironmental Engineering* 134(7): 992-1004.